STATE ALIGNMENT-BASED IMITATION LEARNING

Anonymous authors
Paper under double-blind review

ABSTRACT

Consider an imitation learning problem that the imitator and the expert have different dynamics models. Most of existing imitation learning methods fail because they focus on the imitation of actions. We propose a novel state alignment-based imitation learning method to train the imitator by following the state sequences in the expert demonstrations as much as possible. The alignment of states comes from both local and global perspectives. We combine them into a reinforcement learning framework by a regularized policy update objective. We show the superiority of our method on standard imitation learning settings as well as the challenging settings in which the expert and the imitator have different dynamics models.

1 INTRODUCTION

Learning from demonstrations (imitation learning, abbr. as IL) is a basic strategy to train agents for solving complicated tasks. Imitation learning methods can be generally divided into two categories: behavior cloning (BC) and inverse reinforcement learning (IRL). Behavior cloning (Ross et al., 2011b) formulates a supervised learning problem to learn a policy that maps states to actions using demonstration trajectories. Inverse reinforcement learning (Russell, 1998; Ng et al., 2000) tries to find a proper reward function that can induce the given demonstration trajectories. GAIL (Ho & Ermon, 2016) and its variants (Fu et al., 2017a; Qureshi et al., 2018; Xiao et al., 2019) are the recently proposed IRL-based methods, which uses a GAN-based reward to align the distribution of state-action pairs between the expert and the imitator.

Although state-of-the-art BC and IRL methods have demonstrated compelling performance in standard imitation learning settings, e.g. control tasks (Ho & Ermon, 2016; Fu et al., 2017a; Qureshi et al., 2018; Xiao et al., 2019) and video games (Aytar et al., 2018b), these approaches are developed based on a strong assumption: the expert and the imitator share **the same** dynamics model; specifically, they have the same action space, and any feasible state-action pair leads to the same next state in probability for both agents. The assumption brings severe limitation in practical scenarios: Imagine that a robot with a low speed limit navigates through a maze by imitating another robot which moves fast, then, it is impossible for the slow robot to execute the exact actions as the fast robot. However, the demonstration from the fast robot should still be useful because it shows the path to go through the maze.

We are interested in the imitation learning problem under a relaxed assumption: Given an imitator that shares the same state space with the expert but may have a different dynamics model, we train the imitator to follow the state sequence in expert demonstrations as much as possible. This is a more general formulation since it poses fewer requirements on the experts and makes demonstration collection easier. Due to the dynamics mismatch, the imitator becomes more likely to deviate from the demonstrations compared with the traditional imitation learning setting. Therefore, it is very important that the imitator should be able to resume to the demonstration trajectory by itself. Note that neither BC-based methods nor GAIL-based IRL methods have learned to handle dynamics misalignment and deviation correction.

To address the issues, we propose a novel approach with four main features: 1) *State-based*. Compared to the majority of literature in imitation learning, our approach is state-based rather than action-based. Not like BC and IRL that essentially match state-action pairs between the expert and the imitator, we only match states. An inverse model of the imitator dynamics is learned to recover the action; 2) *Deviation Correction*. A state-based β-VAE (Higgins et al., 2017) is learned as the prior for the next state to visit. Compared with ordinary behavior cloning, this VAE-based next state predictor can advise the imitator to return to the demonstration trajectory when it deviates. The robustness benefits from VAE's latent stochastic sampling; 3) *Global State Alignment*. While the VAE can help the agent to correct its trajectory to some extent, the agent may still occasionally enter

states that are far away from demonstrations, where the VAE has no clue how to correct it. So we have to add a global constraint to align the states in demonstration and imitation. Inspired by GAIL that uses reward to align the distribution of state-action pairs, we also formulate an IRL problem whose maximal cumulative reward is the Wasserstein Distance between states of demonstration and imitation. Note that we choose not to involve state-action pairs as in GAIL(Ho & Ermon, 2016), or state-state pairs as in an observation-based GAIL (Ho & Ermon, 2016), because our state-only formulation imposes weaker constraints than the two above options, thus providing more flexibility to handle different environment dynamics; 4) *Regularized Policy Update*. We combine the prior for next state learned from VAE and the Wasserstein distance-based global constraint from IRL in a unified framework, by imposing a Kullback-Leibler divergence based regularizer to the policy update in the Proximal Policy Optimization algorithm.

To empirically justify our ideas, we conduct experiments in two different settings. We first show that our approach can achieve similar or better results on the standard imitation learning setting, which assumes the same dynamics between the expert and the imitator. We then evaluate our approach in the more challenging setting that the dynamics of the expert and the imitator are different. In a number of control tasks, we either change the physics properties of the imitators or cripple them by changing their geometries. Existing approaches either fail or can only achieve very low rewards, but our approach can still exhibit decent performance. Finally, we show that even for imitation across agents of completely different actuators, it is still possible for the state-alignment based method to work. Surprisingly, a point mass and an ant in MuJoCo(Todorov et al., 2012) can imitate each other to navigate in a maze environment.

Our contributions can be summarized as follows:

- Propose to use a state alignment based method in the imitation learning problems where the expert and the imitator have different dynamics models.
- Propose a local state alignment method based on β-VAE and a global state alignment method based on Wasserstein distance.
- Combine the local alignment and global alignment components into a reinforcement learning framework by a regularized policy update objective.

2 Related work

Imitation learning is widely used in solving complicated tasks where pure reinforcement learning might suffer from high sample complexity, like robotics control (Le et al., 2017; Ye & Alterovitz, 2017; Pathak et al., 2018), autonomous vehicle (Bojarski et al., 2016; Pomerleau, 1989), and playing video game (Hester et al., 2018; Pohlen et al., 2018; Aytar et al., 2018a). Behavioral cloning (Bain & Sommut, 1999) is a straight-forward method to learn a policy in a supervised way. However, behavioral cloning suffers from the problem of compounding errors as shown by Ross & Bagnell (2010), and this can be somewhat alleviated by interactive learning, such as DAGGER Ross et al. (2011b). Another important line in imitation learning is inverse reinforcement learning (Russell, 1998; Ng et al., 2000; Abbeel & Ng, 2004; Ziebart et al., 2008; Fu et al., 2017b), which finds a cost function under which the expert is uniquely optimal.

Since IRL can be connected to min-max formulations, works like GAIL, SAM (Ho & Ermon, 2016; Blondé & Kalousis, 2018) utilize this to directly recover policies. Its connection with GANs (Goodfellow et al., 2014) also lead to f-divergence minimization (Ke et al., 2019; Nowozin et al., 2016) and Wasserstein distance minimization (Xiao et al., 2019).

Increasing works like (Aytar et al., 2018b; Liu et al., 2018; Peng et al., 2018; Torabi et al., 2018a) have aspired to learn from observation alone, which requires training a policy through interactions. Methods like (Torabi et al., 2018b; Edwards et al., 2018) will recover actions from observations, and both have offline training stage. Our work also aims to learn a robust imitating policy using a few interactions online.

3 Backgrounds

Variational Autoencoders Kingma & Welling (2013); Rezende et al. (2014) provides a framework to learn both a probabilistic generative model $p_\theta(\mathbf{x}|\mathbf{z})$ as well as an approximated posterior distribution $q_\phi(\mathbf{z}|\mathbf{x})$. β-VAE is a variant VAE that introduces an adjustable hyperparameter β to the original objective:

$$\mathcal{L}(\theta, \phi; \mathbf{x}, \mathbf{z}, \beta) = \mathbb{E}_{q_\phi(\mathbf{z}|\mathbf{x})}\left[\log p_\theta(\mathbf{x}|\mathbf{z})\right] - \beta D_{KL}\left(q_\phi(\mathbf{z}|\mathbf{x}) \| p(\mathbf{z})\right) \tag{1}$$

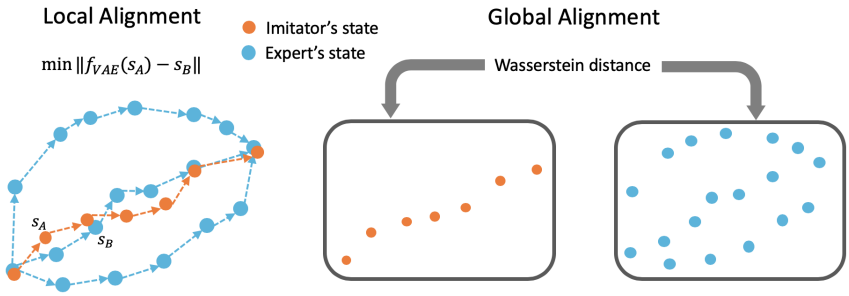

Figure 1: Visualization of state alignment

Larger β will penalize the total correlation (Chen et al., 2018) to encourage more disentangled latent representations, while smaller β often results in sharper and more precise reconstructions.

Wasserstein distance The Wasserstein distance between two density functions $p(x)$ and $q(y)$ with support on a compact metric space (M, d) has an alternative form due to Kantorovich-Rubenstein duality (Villani, 2008):

$$\mathcal{W}(p, q) = \sup_{f \in \mathcal{L}_1} \mathbb{E}_{p(x)}[f(x)] - \mathbb{E}_{q(x)}[f(x)] \tag{2}$$

Here, $\mathcal{L}_1$ is the set of all 1-Lipschitz functions from $\mathcal{M}$ to $\mathbb{R}$.

4 SAIL: State Alignment Based Imitation Learning

4.1 Overview

Our imitation learning method is based on state alignment from both local and global perspectives. For local alignment, the goal is to follow the transition of the demonstration as much as possible, and allow the return to the demonstration trajectory whenever the imitation deviates. To achieve both goals, we use a β-VAE (Higgins et al., 2017) to generate the next state (Figure 1 Left). For global alignment, we set up an objective to minimize the Wasserstein distance between the states in the current trajectory and the demonstrations (Figure 1 Right). There has to be a framework to naturally combine the local alignment and global alignment components. We resort to the reinforcement learning framework by encoding the local alignment as policy prior and encoding the global alignment as reward over states. Using Proximal Policy Optimization (PPO) as the backbone RL solver, we derive a regularized policy update. To maximally exploit the knowledge from demonstrations and reduce interactions with the environment, we adopt a pre-training stage to produce a good initialization based on the same policy prior induced by the local alignment. In the rest parts of this section, we will introduce all the components of our method in details.

4.2 Local Alignment by State Predictive VAE

To align the transition of states locally, we need a predictive model to generate the next state which the agent should target at. And then we can simply train an inverse dynamics model to recover the corresponding action, so as to provide a direct supervision for policy.

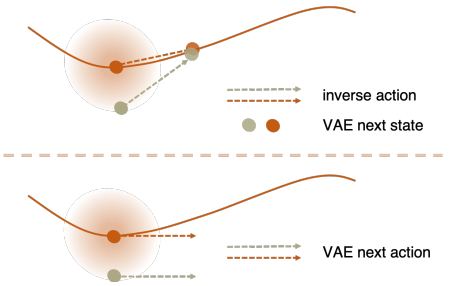

Figure 2: Using VAE as a state predictive model will be more self-correctable because of the stochastic sampling mechanism. But this won't happen when we use VAE to predict actions.

Instead of using an ordinary network to memorize the subsequent states, which will suffer from the same issue of compounding errors as behavioral cloning (Ross & Bagnell, 2010; Ross et al., 2011a), we propose to use VAE to generate the next state based on the following two reasons. First, as shown in (Dai et al., 2018), VAE is more robust to outliers and regularize itself to find the support set of a data manifold, so it will generalize better for unseen data. Second, because of the latent stochastic sampling, the local neighborhood of a data point will have almost the same prediction, which is self-correctable when combined with a precise inverse dynamics model as illustrated in Figure 2.

Algorithm 1 SAIL: State Alignment based Imitation Learning

Require: Expert trajectories $\tau_e \sim \pi_e$, initial policy π, inverse dynamics model g, discriminator ϕ, total episode T, memory capacity S

if Imitator and Expert have the same dynamics model **then**
    Pre-train g using τ_e and random trials
else
    Pre-train g using random trials
end if
Pre-train π using the policy prior ▷ Pre-train Policy Mean and VAE
Pre-train VAE using τ_e
while episode $\leq$ T **do**
    while $|\tau| \leq S$ **do**
        Collect trajectory $\{(s, a, s', r, done)\}$ using π
        Update r using equation 4
        Add $\{(s, a, s', r, done)\}$ to τ
    end while
    Train ϕ using $\max_{\phi \in \mathcal{L}_1} E_{s\sim\tau_e}[\phi(s)] - E_{s\sim\tau}[\phi(s)]$ ▷ Calculate Wasserstein Distance
    Update policy using Equation 5
    Update inverse dynamics model g
end while

We can also use a VAE to generate action based on the current state. But if the agent deviated from the demonstration trajectory a little bit, this predicted action is not necessarily guide the agent back to the trajectory, as shown in Figure 2. And in section 5.3.2, we conduct experiments to compare the state predictive VAE and the action predictive VAE.

Instead of the vanilla VAE, we use β-VAE to balance the KL penalty and prediction error as shown in Eq. 1. In Section 5, we discuss the effects of the hyper-parameter β in different experiment settings.

4.3 Global Alignment by Wasserstein Distance

Due to the difference of dynamics between the expert and the imitator, the VAE-based local alignment cannot fully prevent the imitator from deviating from demonstrations. In such circumstances, we still need to assess whether the imitator is making progress in learning from the demonstrations. We, therefore, seek to control the difference between the state visitation distribution of the demonstration and imitator trajectories, which is a global constraint.

Note that using this global constraint alone will not induce policies that follow from the demonstration. Consider the simple case of learning an imitator from experts of the same dynamics. The expert takes cyclic actions. If the expert runs for 100 cycles with a high velocity and the imitator runs for only 10 cycles with a low velocity within the same time span, their state distribution would still roughly align. That is why existing work such as GAIL aligns state-action occupancy measure. However, as shown later, our state-based distribution matching will be combined with the local alignment component, which will naturally resolve this issue. The advantage of this state-based distribution matching over state-action pair matching as in GAIL or state-next-state pair matching in (Torabi et al., 2018a) is that the constraint becomes loosened.

We use a GAIL-like approach to achieve the state distribution matching by introducing a reinforcement learning problem. Our task is to design the reward to train an imitator that matches the state distribution of the expert.

Before introducing the reward design, we first explain the computation of the Wasserstein distance between the expert trajectories $\{\tau_e\}$ and imitator trajectory $\{\tau\}$ using the Kantorovich duality:

$$\mathcal{W}(\tau_e, \tau) = \sup_{\phi \in \mathcal{L}_1} \mathbb{E}_{s\sim\tau_e}[\phi(s)] - \mathbb{E}_{s\sim\tau}[\phi(s)] \tag{3}$$

The discriminator is trained with a gradient penalty term as WGAN-GP introduced in (Gulrajani et al., 2017)

After the rollout of imitator policy is obtained, the potential ϕ will be updated by Eq 3. Assume a transition among an imitation policy rollout of length T is (s_i, s_{i+1}). We assign the reward as:

$$r(s_i, s_{i+1}) = \frac{1}{T}[\phi(s_{i+1}) - \mathbb{E}_{s\sim\tau_e}\phi(s)] \tag{4}$$

We now explain the intuition of the above reward. By solving equation 3, those states of higher probability in demonstration will have a larger ϕ value. The reward equation 4 will thus encourage the imitator to visit such states.

Maximizing the curriculum reward will be equivalent to

$$J(\pi) = \sum_{t=1}^{T} \mathbb{E}_{s_t, a_t \sim \pi}[r(s_t, a_t)] = \sum_{t=1}^{T} \frac{\mathbb{E}_{s_{t+1}}[\phi(s_{t+1}) - \mathbb{E}_{s \sim \tau_e}[\phi(s)]]}{T} = -\mathcal{W}(\tau_e, \tau)$$

In other words, the optimal policy of this MDP best matches the state visitation distributions w.r.t Wasserstein distance.

4.4 Regularized PPO Policy Update Objective

As mentioned in the second paragraph of Sec 4.3, the global alignment has to be combined with local alignment. This is achieved by adding a prior to the original clipped PPO objective.

We maximize the following objective function:

$$J(\pi_\theta) = L^{CLIP}(\theta) - \lambda D_{KL}\left(\pi_\theta(\cdot|s_t) \middle\| p_a\right) \tag{5}$$

Here, $L^{CLIP}(\theta)$ denotes the clipped surrogate objective used in the original PPO algorithm:

$$L^{CLIP}(\theta) = \hat{\mathbb{E}}_t\left[\min\left(\frac{\pi_\theta(a|s)}{\pi_{\theta_{old}}(a|s)}\hat{A}_t, \text{clip}\left(\frac{\pi_\theta(a|s)}{\pi_{\theta_{old}}(a|s)}, 1-\epsilon, 1+\epsilon\right)\hat{A}_t\right)\right], \tag{6}$$

where $\hat{A}_t$ is an estimator of the advantage function at timestep t. The advantage function is calculated based on a reward function described in Sec 4.3.

The D_{KL} term in equation (5) serves as a regularizer to keep the policy close to a learned policy prior p_a. This policy prior p_a is derived from the state predictive VAE and an inverse dynmaics model as follows.

Assume the inverse dynamics model is $g_{inv}(s_t, s_{t+1}) = a$ and the β-VAE is $f(s_t) = s_{t+1}$. We define the policy prior to be

$$p_a(a_t|s_t) \propto \exp\left(-\left\|\frac{g_{inv}(s_t, f(s_t)) - a_t}{\sigma}\right\|^2\right) \tag{7}$$

where the RHS is a pre-defined policy prior.

4.5 Pre-training

For the pre-training stage, we pretrain the state predictive VAE, the inverse model, and adjust the mean value of π_θ. Practically, we observe that optimizing σ using D_{KL} defined in Eq 5 will cause the variance to grow up to a unreasonable large value. Therefore, we fix the variance of policy and only update the mean to make the policy converge to a meaningful initialization with certain stochasticity.

5 Experiments

We conduct two different kinds of experiments to show the superiority of our method. In Sec 5.1, we compare our method with behavior cloning, GAIL, and AIRL in control setting where the expert and the imitator have different dynamics model, e.g., both of them are ant robots but the imitator has shorter legs. In Sec 5.1, we further evaluate in the traditional imitation learning setting. Finally, in Sec 5.3, we conduct ablation study to show the contribution of the components.

5.1 Imitation Learning across Agents of Different Action Dynamics

5.1.1 Actors of Modified Physics and Geometry Properties

We create environments using MuJoCo (Todorov et al., 2012) by changing some attributes of experts, such as the density and geometry of the body. We choose 2 basic environments, Ant and

Swimmer, and augment them into 6 different environments: Heavy/Light/Disabled Ant/Swimmer. The Heavy/Light agents have modified density, and the disabled agents have modified head/tail/leg lengths. The demonstrations are collected from the standard Ant-v2 and Swimmer-v2. More descriptions of the environments and the demonstration collection process can be founded in the Appendix.

We then evaluate our method on them. Figure 3 demonstrates the superiority of our methods over all the baselines. Our approach is the most stable in all the 6 environments and shows the leading performance in each of them. GAIL seems to be the most sensitive to dynamics difference. AIRL, which is designed to solve imitation learning for actors of different dynamics, can perform on par with our method in two swimmer-based environments (DisabledSwimmer and HeavySwimmer) that have relatively lower dimensional action space (2D for swimmer versus 8D for ants). Interestingly, the stability and performance of vanilla behavior cloning are quite reasonable in 4 of the environments, although it failed to move about in the DisabledAnt and HeavyAnt environments.[1]

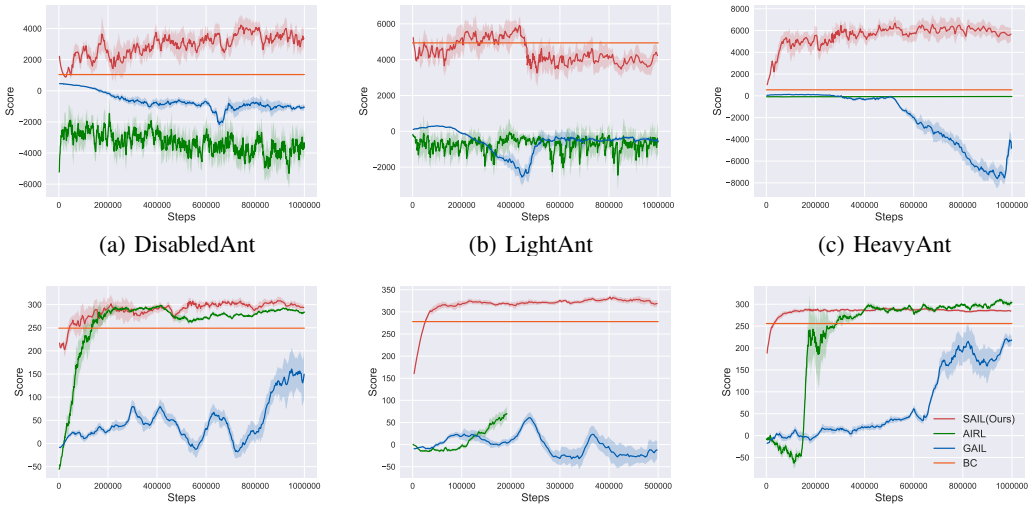

(a) DisabledAnt (b) LightAnt (c) HeavyAnt

(d) DisabledSwimmer (e) LightSwimmer (f) HeavySwimmer

Figure 3: Comparison with BC, GAIL and AIRL when dynamics are different from experts.

5.1.2 Actors of Heterogeneous Action Dynamics

We consider an extremely challenging setting that the imitator and demonstrator are functionally different. One typical example of expert/imitator pair in practice would be a human and a humanoid robot. We consider a much simplified version but with similar nature – a Point and an Ant in MuJuCo. In this task, even the state space cannot be exactly matched, since some of the dimensions of the states describe actor-specific information, such as leg velocity. Nonetheless, there are still some shared dimensions across the state space of the imitator and the actor, e.g., the location of the center of mass, and the demonstration should still teach the imitator in these dimensions.

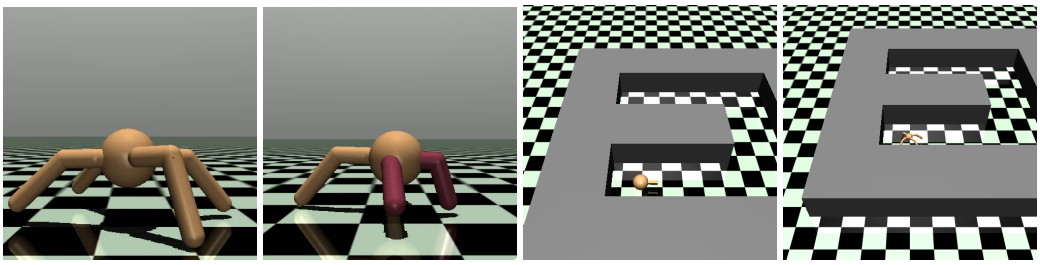

(a) Original Ant (b) Disabled Ant (c) PointMaze (d) AntMaze

Figure 4: Imitation Learning of Actors with Heterogeneous Action Dynamics.

[1]For LightSwimmer 3(e), AIRL meets MuJoCo numerical exception for several trials.

The first task is that the Ant should reach the other side of the maze from several successful demonstrations of a Point robot. As shown in Figure 4(c) and Figure 4(d), the maze structure for the ant and point mass is exactly the same.

We use the similar setting to other hierarchical reinforcement learning methods such as HIRO and Near-Optimal RL (Nachum et al., 2018a;b). The "goal space" is the $x - y$ position, and the first two dimensions of the state space are used to verify whether the agent has reached the goal. To solve this problem, we first pretrain an VAE on the demonstrations, and use this VAE to propose the next "subgoal" for the Ant. The inverse model will take state and goal as input, and generate an action.

Table 1: Compare behavior cloning to variational behavior cloning

β	Environments	
	HalfCheetah-50	Hopper-50
0.1	230.52 $\pm$ 13.26	203.87 $\pm$ 14.39
0.01	1320.04 $\pm$ 15.43	438.10 $\pm$ 20.43
0.001	3306.91 $\pm$ 12.51	3303.72 $\pm$ 10.46
None	**4813.20 $\pm$ 1949.26**	**3525.87 $\pm$ 6.74**

Our performance is shown in Figure 5(c). After 1M training steps, the agent has success rate of 0.8 to reach the other side of the maze.

5.2 Actors of the Same Dynamics (Standard Imitation Learning)

We also evaluate our algorithm on 6 non-trivial control tasks in MuJuCo: Swimmer, Hopper, Walker, Ant, HalfCheetach, and Humanoid. We first collect demonstration trajectories with Soft Actor-Critic, which can learn policies that achieve high scores in most of these environments[2]. For comparison, we evaluate our method against 3 baselines: behavior cloning, GAIL, and AIRL[3]. Also, to create even stronger baselines for the cumulative reward and imitator run-time sample complexity, we initialize GAIL with behavior cloning, which would obtain higher scores in Swimmer and Walker. Lastly, to evaluate how much each algorithm depends on the amount of demonstrations, we sampled demonstration trajectories of ten and fifty episodes.

Table 2 depicts representative results in Hopper and HalfCheetah[4]. Our method after pretraining and before online update can perform similarly to behavior cloning. After online update, our method can obtain higher scores. However, even a strong initialization by behavior cloning cannot ensure GAIL to learn a good policy.

Table 2: Performance on Hopper-v2 and HalfCheetah-v2

	Hopper-v2		HalfCheetah-v2	
# Demo	10	50	10	50
Expert	3566 $\pm$ 1.24		12294.22 $\pm$ 273.59	
BC	1318.76 $\pm$ 804.36	3525.87 $\pm$ 6.74	441.37 $\pm$ 251.31	3613.20 $\pm$ 1949.26
GAIL	3372.66 $\pm$ 130.75	3363.97 $\pm$ 262.77	474.42 $\pm$ 389.30	-175.83 $\pm$ 26.76
BC-GAIL	3132.11 $\pm$ 520.65	3130.82 $\pm$ 554.54	578.85 $\pm$ 934.34	1097.51 $\pm$ 1173.93
AIRL	3.07 $\pm$ 0.02	3.31 $\pm$ 0.02	-146.46 $\pm$ 23.57	755.46 $\pm$ 10.92
Our init	**3412.58 $\pm$ 45.97**	**3601.16 $\pm$ 30.14**	**1064.44 $\pm$ 227.32**	**7102.29 $\pm$ 910.54**
Our final	**3539.56 $\pm$ 13.36**	**3614.19 $\pm$ 15.74**	**1616.34 $\pm$ 180.76**	**8817.32 $\pm$ 860.55**

5.3 Ablation study

5.3.1 Coefficient β in β-VAE

β-VAE introduces an additional parameter to the original VAE. It controls the variance of the randomly sampled latent variable sampling, which subsequently affects the reconstruction quality and robustness. Theoretically, a smaller β leads to better state prediction quality, with the cost of losing the deviation correction ability (Dai et al., 2018).

We evaluate VAE in settings of both the imitator has the same dynamics and has different dynamics. We select HalfCheetah-v2 and HeavyAnt as an example. For HalfCheetah-v2, we pretrain the inverse dynamics and VAE using given demonstrations so that the initial performance will tell the

[2]We collect near-optimal demonstration on Swimmer using TRPO due to the limited performance of SAC.

[3]AIRL and EAIRL have similar performance, and we only compare to AIRL.

[4]Results for other environments can be founded in the Appendix

quality of the VAE's prediction. For DisabledAnt, we pretrain the dynamics with random trials, which results in forward/inverse dynamics estimation of less accuracy. In this case, we examine both its initialized performance and final performance. The results are shown in Table 3. We find out that for β in $[0.01, 0.1]$, the performance is better. Specifically, when the imitator is different from the expert, a smaller β will result in poor performance as it overfits the demonstration data.

We also compare our method with an ordinary MLP trained by MSE loss. We find out that VAE outperforms MLP in all settings. Note that the MLP-based approach is very similar to the state-based behavior cloning work of (Torabi et al., 2018b).

5.3.2 Action Predictive β-VAE

In Figure 2, we mentioned that a VAE to predict the next action is less favorable. To justify the claim, we compare a VAE-based BC with a vanilla BC that both predict actions, as shown in Table 1. Experiments show that VAE-BC is even outperformed by a vanilla BC, especially when β is larger than 0.001, let alone our state-predictive BC.

Table 3: Analyze the role of VAE coefficient. The "None" item means replacing VAE with an ordinary network with linear layers.

β	Environments			
	HalfCheetah-50	HalfCheetah-20	HeavyAnt-Initial	HeavyAnt-Final
0.2	2007.86	1289.21	258.91	282.13
0.15	2653.04	1151.93	1149.65	1502.68
0.1	**7102.29**	1797.44	**1219.34**	**5208.45**
0.05	5933.28	**2215.71**	987.72	4850.62
0.01	5893.17	1982.62	740.54	1921.26
0.005	4415.04	1369.57	320.54	399.31
None	4759.69	1123.79	359.15	-62.13

5.3.3 Effect of Wasserstein Distance and KL regularization

(a) HalfCheetah-v2 (b) Disabled Ant (c) AntMaze

Figure 5: (a), (b) show the effects of Wasserstein distance and KL regularization on HalfCheetah-v2 and Humanoid-v2 given 20 demonstration trajectories. And (c) presents the result on Antmaze.

In our policy update process, we use Wasserstein distance with KL regularization to update the policy. To analyze their effects on the performance, we use HalfCheetah-v2 and Humanoid-v2 with 20 expert trajectories. For each environment, they use the same pretrained inverse model and VAE, thus they have the same behavior after pretraining.

As shown in Figure 5(a),(b), Wasserstein distance combined with KL regularization performs the best. If no Wasserstein distance is provided, due to the existence of policy exploration, although the agent may deviate from the expert trajectories, the KL regularizer can still help to restrict the policy. However, if only the Wasserstein distance is provided, PPO will explore more unfamiliar states, leading to the lowest performance. From Figure 5(a), we can see that HalfCheetah can finally learn to return to the right trajectory with the help of the Wasserstein distance.

6 Conclusion

We proposed SAIL, a flexible and practical imitation learning algorithms that use state alignment from both local and global perspective. We demonstrate the superiority of our method using MuJoCo environments, especially when the action dynamics are different from the demonstrations.

REFERENCES

Pieter Abbeel and Andrew Y Ng. Apprenticeship learning via inverse reinforcement learning. In *Proceedings of the twenty-first international conference on Machine learning*, pp. 1. ACM, 2004.

Yusuf Aytar, Tobias Pfaff, David Budden, Thomas Paine, Ziyu Wang, and Nando de Freitas. Playing hard exploration games by watching youtube. In *Advances in Neural Information Processing Systems*, pp. 2930–2941, 2018a.

Yusuf Aytar, Tobias Pfaff, David Budden, Thomas Paine, Ziyu Wang, and Nando de Freitas. Playing hard exploration games by watching youtube. In *Advances in Neural Information Processing Systems*, pp. 2930–2941, 2018b.

Michael Bain and Claude Sommut. A framework for behavioural cloning. *Machine intelligence*, 15 (15):103, 1999.

Lionel Blondé and Alexandros Kalousis. Sample-efficient imitation learning via generative adversarial nets. *arXiv preprint arXiv:1809.02064*, 2018.

Mariusz Bojarski, Davide Del Testa, Daniel Dworakowski, Bernhard Firner, Beat Flepp, Prasoon Goyal, Lawrence D Jackel, Mathew Monfort, Urs Muller, Jiakai Zhang, et al. End to end learning for self-driving cars. *arXiv preprint arXiv:1604.07316*, 2016.

Tian Qi Chen, Xuechen Li, Roger B Grosse, and David K Duvenaud. Isolating sources of disentanglement in variational autoencoders. In *Advances in Neural Information Processing Systems*, pp. 2610–2620, 2018.

Bin Dai, Yu Wang, John Aston, Gang Hua, and David Wipf. Connections with robust pca and the role of emergent sparsity in variational autoencoder models. *The Journal of Machine Learning Research*, 19(1):1573–1614, 2018.

Ashley D Edwards, Himanshu Sahni, Yannick Schroecker, and Charles L Isbell. Imitating latent policies from observation. *arXiv preprint arXiv:1805.07914*, 2018.

Justin Fu, Katie Luo, and Sergey Levine. Learning robust rewards with adversarial inverse reinforcement learning. *arXiv preprint arXiv:1710.11248*, 2017a.

Justin Fu, Katie Luo, and Sergey Levine. Learning robust rewards with adversarial inverse reinforcement learning. *arXiv preprint arXiv:1710.11248*, 2017b.

Ian Goodfellow, Jean Pouget-Abadie, Mehdi Mirza, Bing Xu, David Warde-Farley, Sherjil Ozair, Aaron Courville, and Yoshua Bengio. Generative adversarial nets. In *Advances in neural information processing systems*, pp. 2672–2680, 2014.

Ishaan Gulrajani, Faruk Ahmed, Martin Arjovsky, Vincent Dumoulin, and Aaron C Courville. Improved training of wasserstein gans. In *Advances in neural information processing systems*, pp. 5767–5777, 2017.

Tuomas Haarnoja, Aurick Zhou, Pieter Abbeel, and Sergey Levine. Soft actor-critic: Off-policy maximum entropy deep reinforcement learning with a stochastic actor. *arXiv preprint arXiv:1801.01290*, 2018.

Todd Hester, Matej Vecerik, Olivier Pietquin, Marc Lanctot, Tom Schaul, Bilal Piot, Dan Horgan, John Quan, Andrew Sendonaris, Ian Osband, et al. Deep q-learning from demonstrations. In *Thirty-Second AAAI Conference on Artificial Intelligence*, 2018.

Irina Higgins, Loic Matthey, Arka Pal, Christopher Burgess, Xavier Glorot, Matthew Botvinick, Shakir Mohamed, and Alexander Lerchner. beta-vae: Learning basic visual concepts with a constrained variational framework. *ICLR*, 2(5):6, 2017.

Jonathan Ho and Stefano Ermon. Generative adversarial imitation learning. In *Advances in neural information processing systems*, pp. 4565–4573, 2016.

Liyiming Ke, Matt Barnes, Wen Sun, Gilwoo Lee, Sanjiban Choudhury, and Siddhartha Srinivasa. Imitation learning as f-divergence minimization. *arXiv preprint arXiv:1905.12888*, 2019.

Diederik P Kingma and Max Welling. Auto-encoding variational bayes. *arXiv preprint arXiv:1312.6114*, 2013.

Hoang M Le, Yisong Yue, Peter Carr, and Patrick Lucey. Coordinated multi-agent imitation learning. In *Proceedings of the 34th International Conference on Machine Learning-Volume 70*, pp. 1995–2003. JMLR. org, 2017.

YuXuan Liu, Abhishek Gupta, Pieter Abbeel, and Sergey Levine. Imitation from observation: Learning to imitate behaviors from raw video via context translation. In *2018 IEEE International Conference on Robotics and Automation (ICRA)*, pp. 1118–1125. IEEE, 2018.

Ofir Nachum, Shixiang Gu, Honglak Lee, and Sergey Levine. Near-optimal representation learning for hierarchical reinforcement learning. *arXiv preprint arXiv:1810.01257*, 2018a.

Ofir Nachum, Shixiang Shane Gu, Honglak Lee, and Sergey Levine. Data-efficient hierarchical reinforcement learning. In *Advances in Neural Information Processing Systems*, pp. 3303–3313, 2018b.

Andrew Y Ng, Stuart J Russell, et al. Algorithms for inverse reinforcement learning. In *Icml*, volume 1, pp. 2, 2000.

Sebastian Nowozin, Botond Cseke, and Ryota Tomioka. f-gan: Training generative neural samplers using variational divergence minimization. In *Advances in neural information processing systems*, pp. 271–279, 2016.

Deepak Pathak, Parsa Mahmoudieh, Michael Luo, Pulkit Agrawal, Dian Chen, Fred Shentu, Evan Shelhamer, Jitendra Malik, Alexei A Efros, and Trevor Darrell. Zero-shot visual imitation. *international conference on learning representations*, 2018.

Xue Bin Peng, Angjoo Kanazawa, Jitendra Malik, Pieter Abbeel, and Sergey Levine. Sfv: Reinforcement learning of physical skills from videos. *ACM Trans. Graph.*, 37(6), November 2018.

Tobias Pohlen, Bilal Piot, Todd Hester, Mohammad Gheshlaghi Azar, Dan Horgan, David Budden, Gabriel Barth-Maron, Hado van Hasselt, John Quan, Mel Večerík, et al. Observe and look further: Achieving consistent performance on atari. *arXiv preprint arXiv:1805.11593*, 2018.

Dean A Pomerleau. Alvinn: An autonomous land vehicle in a neural network. In *Advances in neural information processing systems*, pp. 305–313, 1989.

Ahmed H Qureshi, Byron Boots, and Michael C Yip. Adversarial imitation via variational inverse reinforcement learning. *arXiv preprint arXiv:1809.06404*, 2018.

Danilo Jimenez Rezende, Shakir Mohamed, and Daan Wierstra. Stochastic backpropagation and approximate inference in deep generative models. *arXiv preprint arXiv:1401.4082*, 2014.

Stéphane Ross and Drew Bagnell. Efficient reductions for imitation learning. In *Proceedings of the thirteenth international conference on artificial intelligence and statistics*, pp. 661–668, 2010.

Stéphane Ross, Geoffrey Gordon, and Drew Bagnell. A reduction of imitation learning and structured prediction to no-regret online learning. In *Proceedings of the fourteenth international conference on artificial intelligence and statistics*, pp. 627–635, 2011a.

Stéphane Ross, Geoffrey Gordon, and Drew Bagnell. A reduction of imitation learning and structured prediction to no-regret online learning. In *Proceedings of the fourteenth international conference on artificial intelligence and statistics*, pp. 627–635, 2011b.

Stuart J Russell. Learning agents for uncertain environments. In *COLT*, volume 98, pp. 101–103, 1998.

John Schulman, Sergey Levine, Pieter Abbeel, Michael Jordan, and Philipp Moritz. Trust region policy optimization. In *International Conference on Machine Learning*, pp. 1889–1897, 2015.

Emanuel Todorov, Tom Erez, and Yuval Tassa. Mujoco: A physics engine for model-based control. In *2012 IEEE/RSJ International Conference on Intelligent Robots and Systems*, pp. 5026–5033. IEEE, 2012.

Faraz Torabi, Garrett Warnell, and Peter Stone. Generative adversarial imitation from observation. *arXiv preprint arXiv:1807.06158*, 2018a.

Faraz Torabi, Garrett Warnell, and Peter Stone. Behavioral cloning from observation. *arXiv preprint arXiv:1805.01954*, 2018b.

Cédric Villani. *Optimal transport: old and new*, volume 338. Springer Science & Business Media, 2008.

Huang Xiao, Michael Herman, Joerg Wagner, Sebastian Ziesche, Jalal Etesami, and Thai Hong Linh. Wasserstein adversarial imitation learning. *arXiv preprint arXiv:1906.08113*, 2019.

Gu Ye and Ron Alterovitz. Guided motion planning. In *Robotics research*, pp. 291–307. Springer, 2017.

Brian D Ziebart, Andrew Maas, J Andrew Bagnell, and Anind K Dey. Maximum entropy inverse reinforcement learning. 2008.

A LEARNING ACROSS DIFFERENT ENVIRONMENTS

PointMaze & AntMaze As shown in Figure 4, a point mass or an ant is put in a 24×24 U-maze. The task is to make the agent reach the other side of U-maze with the demonstration from the point mass. The ant is trained to reach a random goal in the maze from a random location, and should reach the other side of the maze. The state space of ant is 30-dim, which contains the positions and velocities.

HeavyAnt Two times of original Ant's density.

LightAnt One tenth of original Ant's density.

DisabledAnt Two front legs are 3 quarters of original Ant's legs.

HeavySwimmer 2.5 times of original Swimmer's density.

LightSwimmer One twentieth of original Swimmer's density.

DisabledSwimmer Make the last joint 1.2 times longer and the first joint 0.7 times of the original length

The exact results of these environments are listed in Table 4, 5. All the statistics are calculated from 20 trails.

Table 4: Performance on modifeid Swimmer

	DisabledSwimmer	LightSwimmer	HeavySwimmer
BC	249.09 $\pm$ 1.53	277.99 $\pm$ 3.41	255.95 $\pm$ 2.5
GAIL	228.46 $\pm$ 2.02	-4.11 $\pm$ 0.51	254.91 $\pm$ 1.35
AIRL	283.42 $\pm$ 3.69	67.58 $\pm$ 25.09	**301.27 $\pm$ 5.21**
SAIL(Ours)	**287.71 $\pm$ 2.31**	**342.61 $\pm$ 6.14**	286.4 $\pm$ 3.2

Table 5: Performance on modified Ant

	DisabledAnt-v0	HeavyAnt-v0	LightAnt-v0
BC	1042.45 $\pm$ 75.13	550.6 $\pm$ 77.62	**4936.59 $\pm$ 53.42**
GAIL	-1033.54 $\pm$ 254.36	-1089.34 $\pm$ 174.13	-971.74 $\pm$ 123.14
AIRL	-3252.69 $\pm$ 153.47	-62.02 $\pm$ 5.33	-626.44 $\pm$ 104.31
SAIL(Ours)	**3305.71 $\pm$ 67.21**	**5608.47 $\pm$ 57.67**	4335.46 $\pm$ 82.34

B IMITATION BENCHMARK EXPERIMENTS SETTINGS AND RESULTS

We use six MuJoCo (Todorov et al., 2012) control tasks. The name and version of the environments are listed in Table 6, which also list the state and action dimension of the tasks with expert performance and reward threshold to indicate the minimum score to solve the task. All the experts are trained by using SAC (Haarnoja et al., 2018) except Swimmer-v2 where TRPO (Schulman et al., 2015) get higher performance.

Table 6: Performance on benchmark control tasks

Environment	State Dim	Action Dim	Reward threshold	Expert Performance
Swimmer-v2	8	2	360	332
Hopper-v2	11	3	3800	3566
Walker2d-v2	17	6	-	4924
Ant-v2	111	8	6000	6157
HalfCheetah-v2	17	6	4800	12294
Humanoid-v2	376	17	1000	5187

The exact performance of all methods are list in Table 7, 8, 9, 10, 11, 12. We compare GAIL(Ho & Ermon, 2016), behavior cloning, GAIL with behavior cloning initilization and AIRL to our method containing. Means and standard deviations are calculated from 20 trajectories after the agents converge and the number total interactions with environments is less than one million environment steps.

Table 7: Performance on Swimmer-v2 with different trajectories

Swimmer-v2				
#Demo	5	10	20	50
Expert	332.88 ± 1.24			
BC	328.85 ± 2.26	331.17 ± 2.4	332.17 ± 2.4	330.65 ± 2.42
GAIL	304.64 ± 3.16	271.59 ± 11.77	56.16 ± 5.99	246.73 ± 5.76
BC-GAIL	313.80 ± 3.42	326.58 ± 7.87	294.93 ± 12.21	315.68 ± 9.99
AIRL	332.11 ± 2.57	338.43 ± 3.65	335.67 ± 2.72	**340.08 ± 2.70**
Our init	**332.36 ± 3.62**	335.78 ± 0.34	**336.23 ± 2.53**	334.03 ± 2.11
Our final	**336.22 ± 3.23**	**339 ± 3.21**	**339 ± 1.87**	336.31 ± 3.20

Table 8: Performance on Hopper-v2 with different trajectories

Hopper-v2				
#Demo	5	10	20	50
Expert	3566 ± 1.24			
BC	1471.40 ± 637.25	1318.76 ± 804.36	1282.46 ± 772.24	3525.87 ± 6.74
GAIL	3300.32 ± 331.61	3372.66 ± 130.75	3201.97 ± 295.27	3363.97 ± 262.77
BC-GAIL	**3122.23 ± 358.65**	3132.11 ± 520.65	3111.42 ± 414.28	3130.82 ± 554.54
AIRL	4.12 ± 0.01	3.07 ± 0.02	4.11 ± 0.01	3.31 ± 0.02
Our init	2322.49 ± 30.93	**3412.58 ± 45.97**	**3314.03 ± 31.32**	**3601.16 ± 30.14**
Our final	3092.26 ± 67.72	**3539.56 ± 13.36**	**3516.81 ± 28.98**	**3614.19 ± 15.74**

Table 9: Performance on Walker2d-v2 with different trajectories

Walker2d-v2				
#Demo	5	10	20	50
Expert	5070.97 ± 209.19			
BC	1617.34 ± 693.63	4425.50 ± 930.62	4689.30 372.33	4796.24 490.05
GAIL	1307.21 ± 388.55	692.16 ± 145.34	1991.58 446.66	751.21 150.18
BC-GAIL	**3454.91 ± 792.40**	2094.68 ± 1425.05	3482.31 828.21	2896.50 828.18
AIRL	-7.13 ± 0.11	-7.39 ± 0.09	-3.74 ± 0.13	-4.64 ± 0.09
Our init	1859.10 ± 72.44	2038.90 ± 26.78	**4509.82 ± 147.65**	**4757.58 ± 88.45**
Our final	2681.20 ± 53.67	**3764.14 ± 47.01**	**4778.82 ± 76.34**	**4950.73 ± 36.66**

Table 10: Performance on Ant-v2 with different trajectories

Ant-v2				
#Demo	5	10	20	50
Expert	6190.90 ± 254.18			
BC	**3958.20 ± 661.28**	3948.88 ± 753.41	5424.01 ± 473.05	5852.79 ± 572.97
GAIL	340.02 ± 59.02	335.25 ± 89.19	314.35 ± 52.13	284.18 ± 32.40
BC-GAIL	-1081.30 ± 673.65	-1177.27 ± 618.67	-13618.45 ± 4237.79	-1166.16 ± 1246.79
AIRL	-839.32 ± -301.54	-386.43 ± 156.98	-586.07 ± 145.43	-393.90 ± 145.13
Our init	1150.82 ± 20.87	3015.43 ± 30.70	5200.58 ± 87.74	5849.88 ± 89.56
Our final	1693.59 ± 35.74	**4983.34 ± 25.99**	**5980.37 ± 42.16**	**5988.65 ± 47.03**

Table 11: Performance on HalfCheetah-v2 with different trajectories

HalfCheetah-v2				
#Demo	5	10	20	50
Expert	12294.22 ± 208.41			
BC	225.42 ± 147.16	441.37 ± 251.31	2782.76 ± 959.67	4813.20 ± 1949.26
GAIL	-84.92 ± 43.29	74.42 ± 389.30	-116.70 ± 34.14	-175.83 ± 26.75
BC-GAIL	1362.59 ± 1255.57	578.85 ± 934.34	3744.32 ± 1471.90	1597.50 ± 1173.93
AIRL	**782.36 ± 48.98**	-146.46 ± 23.57	1437.25 ± 25.45	755.46 ± 10.92
Our init	267.71 ± 90.38	**1064.44 ± 227.32**	3200.80 ± 520.04	**7102.74 ± 91.58**
Our final	513.66 ± 15.31	**1616.34 ± 180.76**	**6059.27 ± 344.41**	**8817.32 ± 860.55**

Table 12: Performance on Humanoid-v2 with different trajectories

Humanoid-v2				
#Demo	5	10	20	50
Expert	5286.21 $\pm$ 145.98			
BC	**1521.55$\pm$ 272.14**	**3491.07$\pm$ 518.64**	4686.05 $\pm$355.74	4746.88 $\pm$605.61
GAIL	485.92$\pm$ 27.59	486.44 $\pm$27.18	477.15$\pm$ 22.07	481.14$\pm$ 24.37
BC-GAIL	363.68 $\pm$44.44	410.03 $\pm$33.07	487.99$\pm$ 30.77	464.91 $\pm$33.21
AIRL	79.72 $\pm$ 4.27	87.15 $\pm$ 5.01	-1293.86 $\pm$ 10.70	84.84 $\pm$ 6.46
Our init	452.31 $\pm$ 19.12	1517.63 $\pm$ 11.45	4610.25 $\pm$ 275.86	**4776.83 $\pm$ 132.46**
Our final	1225.58 $\pm$ 21.88	2190.43 $\pm$ 28.18	**4716.91 $\pm$68.29**	4790.07 $\pm$ 70.01

C HYPER-PARAMETER AND NETWORK ARCHITECTURE

When we pretrain the policy network with our methods, we choose $\beta = 0.05$ in β-VAE. We use Adam with learning rate 3e-4 as the basic optimization algorithms for all the experiments. The policy network and value network used in the algorithms all use a three-layer relu network with hidden size 128. All the algorithms are trained by using about one million environment interactions. All the statistics are calculated with twenty trails.